Cardiovascular Diabetology

RESEARCH

Open Access

Sacubitril/Valsartan partially alleviates myocardial infarction injury by activating the FGF21 signaling pathway via PPARs

Wenjuan Wei[1†], Guangsen Xu[2†], Jiaer Gao[1], Guiyun Wang[2], Ye Wang[2], Caiyan Li[1], Junwei Zheng[2], Huiying Lu[2], Yunyan Lu[1], Kun Wang[2], Hongtao Xu[3], Cong Wang[2*] and Xuebo Pan[1,2*]

Abstract

The recent discovery of clinically significant data, alongside novel physiological and pathological occurrences surrounding sacubitril/valsartan (Sac/Val) beyond its approved indications, necessitates an urgent reevaluation of its underlying mechanism of action. In the present investigation, we observed a substantial elevation in the serum levels of fibroblast growth factor 21 (FGF21) among patients with acute myocardial infarction (AMI) who were administered Sac/Val, compared to those who were not, utilizing ELISA-based measurements. Furthermore, through the utilization of a mouse model of myocardial infarction induced by ligation of the left anterior descending branch, we confirmed that FGF21 mediates the cardioprotective effect of Sac/Val, employing both loss-of-function and gain-of-function approaches. Molecular docking and SPR experiments validated that Sac/Val can regulate FGF21 via its interaction with PPARs, and verified the role of PPARs in mediating Sac/Val regulation of FGF21 by inhibiting PPARs. In conclusion, we found that Sac/Val can act as an agonist of FGF21, which provides a new idea for the development of FGF21 drugs, and FGF21 as a new target of Sac/Val to ameliorate myocardial infarction, which provides a basis for new indications for Sac/Val.

Keywords Sacubitril/Valsartan, Fibroblast growth factor 21, Peroxisome proliferation-activated receptor alpha, Peroxisome proliferation-activated receptor gamma, Myocardial infarction

Introduction

Acute myocardial infarction (AMI) remains a significant global health burden, accounting for approximately one-third of clinical deaths in developed nations and standing as the primary cause of mortality and morbidity worldwide [1]. AMI often leads to heart failure, arrhythmias, and various other comorbidities, necessitating multifaceted treatment strategies to mitigate the risk of cardiac death and post-infarction complications. Among these strategies, reperfusion therapy and pharmacological interventions are paramount in the management of AMI [2]. While reperfusion therapy has gained widespread clinical acceptance, pharmacological treatments remain equally crucial.

†Wei Wenjuan and Xu Guangsen have contributed equally to this work.

*Correspondence:
Cong Wang
cwang@wmu.edu.cn
Xuebo Pan
xuebopan@wmu.edu.cn
[1]Department of Clinical Research, The First People's Hospital of Xiaoshan District, Xiaoshan Affiliated Hospital of Wenzhou Medical University, Hangzhou 311200, Zhejiang, China
[2]School of Pharmaceutical Sciences, Wenzhou Medical University, University Town, Wenzhou 325035, Zhejiang, China
[3]Lishui Central Hospital, The Fifth Hospital Affiliated to Wenzhou Medical University, LiShui 323000, Zhejiang, China

Recently, the angiotensin receptor-neprilysin inhibitor (ARNI) Sacubitril/Valsartan (Sac/Val) has garnered increasing interest in treating cardiac diseases. Although no statistical difference was achieved for the primary trial outcome in the PARADISE-MI trial, the risk of the primary endpoint events (cardiovascular death, first heart failure hospitalization, and outpatient progression to heart failure) was reduced by 10% in the ARNI group compared with the ramipril group. Thus Sac/Val remains an excellent drug for improving myocardial infarction [3]. In other heart diseases, several animal studies have also shown promising cardioprotective effects of Sac/Val post-MI [4–6]. However, the underlying mechanisms of how Sac/Val ameliorates cardiac fibrosis and oxidative stress following MI remain under-explored, necessitating further investigation.

Fibroblast growth factor 21 (FGF21), a distinctive member of the FGF superfamily that belongs to the FGF19 subgroup, holds significant regulatory functions in metabolic processes. Notably, it plays a pivotal role in the pathogenesis of various diseases, including non-alcoholic fatty liver disease (NAFLD), obesity, atherosclerosis and hypertension etc. In cardiovascular diseases, FGF21 exhibits anti-oxidative stress, anti-apoptotic, and anti-fibrotic effects, thereby conferring cardio-protection [7–10]. After MI, liver-derived FGF21 and autocrine FGF21 from the heart collaboratively safeguards the myocardium from further injury [11, 12].

In the current study, we observed a noteworthy correlation between FGF21 and the therapeutic benefits of Sac/Val in patients with MI. To delve deeper into this association, we investigated the link between MI improvement and FGF21 expression in a MI model using wild-type (WT) mice, FGF21 knockout (FGF21KO) mice, and FGF21-overexpressing mice. A large number of studies have now reported that FGF21 can be involved in cardiovascular events through the mediation of Activation of peroxisome proliferator-activated receptors (PPARs) [13–17]. Furthermore, we examined whether this association is facilitated through PPARs signaling. Our results indicate that Sac/Val functions as an agonist of FGF21, and its therapeutic efficacy in treating MI is mediated by PPARs, particularly via the FGF21/PI3K/AKT/mTOR signaling pathway. This investigation offers novel perspectives on the potential role of FGF21 and Sac/Val in MI therapy, opening new avenues for exploring their therapeutic potential in cardiovascular diseases.

Materials and methods

Study population

All participating subjects provided written informed consent, and the study received approval from the Human Ethics Committee of Hangzhou Xiaoshan First People's Hospital. The prospective study cohort was compiled from the hospital's registry of patients, adhering to strict inclusion and exclusion criteria. Inclusion criteria included: (i) patients aged between 18 and 85 years, (ii) patients with an ejection fraction of 50% or less, and (iii) patients with a ProBNP level of 600 ng/L or higher (iv) Patients with ST-segment elevation or non-ST-segment elevation acute myocardial infarction and heart failure. The exclusion criteria were as follows: (i) patients who had used Sac/Val or similar drugs within the past six months, (ii) patients with renal insufficiency, defined as a blood creatinine level of 256 μM or higher, (iii) patients with obesity, having a body mass index (BMI) of 28.0 or higher, (iv) patients with hepatic insufficiency, (v) patients with menstrual disorders, and (vi) patients with tumors, severe infections, autoimmune diseases, or other significant comorbidities. Ultimately, 83 patients met the eligibility criteria and were enrolled in the study, all of whom had myocardial infarction. Of these, 31 patients received Sac/Val treatment, 52 patients did not. We also recruited 28 normal healthy individuals and used them as negative controls. Normal healthy individuals were examined for BMI, cTnT, ProBNP, CK-MB, ejection fraction, left ventricular end-diastolic internal diameter (LVDD), hemoglobin, total cholesterol, triglycerides, fasting glucose, creatinine, and albumin, which were all within the normal range of values, and did not have a history of smoking, alcohol consumption, or a history of hypertension or diabetes. Only blood samples were collected and used for all patients, and no medical interventions were involved. The project was reviewed by the Ethics Committee of the First People's Hospital of Xiaoshan District, Hangzhou.

Mice

The heterozygous *fgf21* mice, kindly donated by Professor Aimin Xu of the University of Hong Kong, underwent heterozygous amplification through breeding with C57BL/6J wild-type mice. Subsequently, FGF21 heterozygous males and females were selectively mated for several consecutive generations to achieve a genetically homogeneous line of FGF21KO homozygous mice, as well as a control line of wild-type (WT) mice. The experimental mice were individually housed in a specific-pathogen-free (SPF) facility within the Animal Experiment Center of Wenzhou Medical University. The housing conditions were strictly maintained, with room temperature set at 22 ± 1 °C, humidity at 60%, and a 12-hour light/12-hour dark cycle. All animal procedures and studies were conducted in accordance with the ethical guidelines approved by the Animal Research Ethics Committee of Wenzhou Medical University.

Animal procedures

Animal procedures were granted by the Animal Research Ethics Committee of Wenzhou Medical University

following the recommendations in the Guide for the Care and Use of Laboratory Animals of the NIH guidelines. To anaesthetize mice, xylazine (10 mg/kg body weight) and ketamine (100 mg/kg) (Phoenix Scientific, Inc., St. Joseph, MO, USA) were intraperitoneally given. To sacrifice mice, asphyxiation of CO_2 was used. (Infuse CO_2 into the box at a rate of 10-30% per minute to replace the euthanasia box and determine that the mice are immobile, not breathing, and have dilated pupils. Turn off the CO_2. observe for an additional 2 min to determine that the mice are dead.)

MI mouse model

To induce MI in male mice aged 10 to 12 weeks, a permanent ligation of the left anterior descending coronary artery was performed. The procedure was initiated by anesthetizing the mice with 2% isoflurane. Following anesthesia, a small incision was made in the left thoracic region at the fourth intercostal space to expose the heart. The left anterior descending coronary artery was precisely located and subsequently ligated, approximately 3 mm distal to the lower margin of the left atrial appendage, using a 6 – 0 silk suture. Immediately after ligation, the heart was carefully repositioned within the chest cavity, and the thoracic cavity was manually evacuated of air. The muscle and skin layers were then sutured in a secure manner to close the incision. Sham surgery was conducted following the same steps, omitting the ligation of the coronary artery. The hearts of mice were divided into infarcted, near-infarcted non-infarcted areas, near-infarcted areas were used for Western Blot, immunohistochemistry, and DHE staining, and infarcted areas were used for H&E and Masson staining. The infarcted area, near-infarcted area, and non-infarcted area were distinguished primarily based on visual observation: upon excision of the heart, the infarcted area appeared pale or grayish, contrasting sharply with the normal myocardium; the near-infarcted area, located between the infarcted and non-infarcted areas, was slightly less distinct but retained some tissue integrity; the non-infarcted area exhibited normal color and intact myocardial structure [18, 19].

Drug administration

In the clinical research section, the use of Sac/Val was based on the Chinese Heart Failure Diagnosis and Treatment Guidelines and was strictly administered in accordance with its recommendations [20]. According to the guidelines, Sac/Val is one of the recommended treatment options for heart failure, specifically indicated for patients with NYHA class II/III heart failure with reduced ejection fraction (HFrEF). For patients with NYHA class II/III HFrEF who remain symptomatic despite treatment with ACEIs/ARBs, ARNI is recommended as a replacement for ACEIs/ARBs to further reduce the incidence and mortality of heart failure. The use of Sac/Val is determined by physicians based on individual patient conditions and clinical judgment, with the medication administered twice daily, in the morning and evening.

In the conduct of our animal experiments, we administered a daily dose of 52 mg/kg of Sac/Val, comprising an equimolar mixture of 26 mg/kg of Val and 26 mg/kg of Sac daily. This dose was deemed comparable to the low-dose regimen, which is also referred to as 1× or low dose, containing 26 mg/kg of Val and Sac each per day. Drug and saline control administrations were performed via once-daily oral gavage, with all solutions being sterile filtered prior to administration. The day before the surgery we gave the mice a once-daily gavage administration, and on the day of the surgery we did not give the drug in order to facilitate the mice's recovery. Therefore, on the day after the surgery, we gave the mice two gavage administrations, and from the third day until the end of the 14 days, we resumed the once-a-day gavage administration. The drugs were procured from MedChemExpress.

Mice that were required to receive PPARs were kept at the same frequency of administration as those receiving Sac/Val, and were injected by intraperitoneal injection of PPARγ antagonist GW9662 or PPARα antagonist GW9662 (1 mg/kg/day, MCE Company, China) or saline after each gavage of Sac/Val.

Measurement of echocardiographic and histological staining

The cardiac physiological functions were rigorously assessed using a Doppler echocardiography system (VINNO 6 VET, VINNO, China). The transthoracic 2D M-mode echocardiographic system was employed to capture M-mode tracings, from which the following parameters were quantified: left ventricle internal dimension in systole (LVIDS), left ventricle internal dimension in diastole (LVIDD), ejection fraction (EF), and fractional shortening (FS, calculated as FS = (LVIDD – LVIDS)/LVIDD × 100%). These measurements were taken in mice anesthetized with 1.5% isoflurane.

To determine the infarct volume, heart samples were fixed in 4% paraformaldehyde for 48–72 h and subsequently embedded in paraffin. Thin slices (5 μm thick) were then prepared and stained using Masson's trichrome or hematoxylin and eosin (H&E) staining. The infarct ratio was analyzed using the ImageJ software and expressed as the volume fraction of collagen (CVF% = collagen area/tissue total area × 100%).

Additionally, cardiac tissues were embedded in the Tissue-Tek OCT compound (Sakura Finetek, Tokyo, Japan) and sectioned serially to a thickness of 10 μm. These cryosections were stained with the superoxide-sensitive

dye DHE (10μM in 0.01% DMSO) and incubated for 30 min at 37 °C in a humidified dark chamber.

Immunohistochemistry (IHC)

Immunohistochemical analysis was conducted to quantify the expression levels of AT1R and Neprilysin. Initially, the tissue sections were dewaxed and hydrated using 10 mM sodium citrate buffer to facilitate antigen retrieval. Subsequently, endogenous peroxidase activity was blocked by incubating the sections for 30 min at room temperature. Following this, 30 μL of normal non-immune animal serum was added dropwise to the sections, which were then washed three times with PBST. The sections were then incubated overnight at 4 °C with the primary antibody. After two washes with PBS, the slides were incubated with a goat anti-rabbit horseradish peroxidase-conjugated secondary antibody for 30 min at room temperature. This incubation step was followed by thorough washing. Finally, the sections were incubated with 3,3'-diaminobenzidine (DAB) for visualization and counterstained with hematoxylin.

Western blotting

Proteins were extracted from cells and various mouse tissues, and subsequently underwent sodium dodecyl sulfate-polyacrylamide gel electrophoresis (SDS-PAGE) for separation. The separated proteins were then transferred onto polyvinylidene difluoride (PVDF) membranes. For Western blotting analysis, horseradish peroxidase-conjugated rabbit anti-IgG was employed as the secondary antibody. The primary antibodies used in this study were FGF21 (ab171941), FGFR1 (ab76464), PPARα (WL00978), PPARγ (ab178860), PI3K (WL00978), p-PI3K (ab182651), AKT (ab179463), p-AKT (ab192623), mTOR (ab134903), p-mTOR (ab109268), Collagen-I (ab138492), α-SMA (ab124964), HIF-1α (ab1), AT1R (ab124505), and Neprilysin (18008-1-AP). The protein bands were visualized using enhanced chemiluminescence (ECL) reagents and their intensities were quantified using ImageJ software.

Enzyme-linked immunosorbent assay

Plasma samples were obtained from mice and patients, and were subsequently stored at −80 °C for further analysis. To determine the concentrations of FGF21, we employed either a mouse-specific ELISA kit (MFG037, Hong Kong) or a human-specific ELISA kit (SHFT09, Hong Kong), strictly adhering to the manufacturer's recommended protocols.

Cell culture and treatment

H9C2 cells, procured from the Cell Bank of the Chinese Academy of Sciences in Shanghai, China, were maintained in a culture medium comprising high-glucose Dulbecco's Modified Eagle Medium (DMEM) from GIBCO, USA. This medium was supplemented with 1% cyan streptomycin double-antibody and 10% (v/v) fetal bovine serum (FBS). The cells were incubated at 37 °C in a controlled atmosphere containing 5% CO_2. To mimic hypoxic injury, the H9C2 cells were exposed to a three-gas incubator for 12 h, where the internal environment consisted of 1% O_2, 5% CO_2, 94% N_2, maintained at a temperature of 37 °C.

AML-12 cells, also obtained from the Cell Bank of the Chinese Academy of Sciences in Shanghai, China, were cultured in F-12 Dulbecco's Modified Eagle Medium (DMEM) from GIBCO, USA. This medium was similarly supplemented with 1% cyan streptomycin double-antibody and 10% (v/v) FBS. The cells were maintained under standard culture conditions of 37 °C and 5% CO_2.

In silico molecular modeling studies

Utilizing the fundamental 'lock-and-key' paradigm governing the interplay between ligands and receptors, the molecular docking approach was employed to scrutinize the interaction dynamics between a small molecule ligand and a biomacromolecule receptor. The initial three-dimensional (3D) structural framework was delineated based on molecular data obtained from PubChem, thus providing a robust foundation for further computational investigations.

SPR measurements

The binding affinity of Sacubitril and Valsartan towards the ligand-binding domains (LBDs) of PPARγ and PPARα was assessed using surface plasmon resonance (SPR) technology, specifically utilizing the Biacore 3000 instrument (Little Chalfont, Buckinghamshire, UK). Prior to immobilization, the target proteins were diluted in 10 mmol/L sodium acetate buffer (pH 4.5) to a final concentration of 0.10 mg/mL. Subsequently, a standard amine-coupling procedure was employed to covalently bind these proteins to CM5 chips. The small molecule compounds were diluted in 1X PBS-P + buffer containing 2% DMSO. The flow rate was set at 30 μL/min, and gradient-diluted solutions of the small molecule compounds were sequentially injected into the flow channel for interaction with the protein immobilized on the chip. The resulting binding data were analyzed using the 1:1 Langmuir binding model to determine the equilibrium dissociation constant (KD) of each compound.

Statistical analysis

All statistical analyses were conducted using GraphPad Prism 8 software (GraphPad, San Diego, CA). To determine significant differences between two groups, an independent samples t-test was employed. For comparing multiple groups, one-way ANOVA along with Tukey's

post hoc test were used to compare difference among groups. To compare the usage rates of other medications between Sac/Val and non-Sac/Val groups, the Chi-Square test was utilized; for medications with low incidence, Fisher's exact test was applied. Additionally, Pearson's correlation analyses were performed to investigate the potential associations between serum FGF21 levels and other relevant parameters. The threshold for statistical significance was set at $p < 0.05$, while $p < 0.01$ was considered indicative of a highly significant relationship.

Table 1 Sociodemographic and clinical characteristics of the 83 subjects related to 2021–2023 according to MI vs. MI + Sac/Val

	AMI	AMI + Sac/Val	*P* value
Sample size n (%)	52(62.65%)	31(37.35%)	
Age, in years, mean ± SD	60.22 ± 12.31	60.77 ± 15.03	0.8570
BMI, mean ± SD (kg/m2)	23.50 ± 2.78	24.45 ± 2.43	0.1482
Hemoglobin, mean ± SD (g/L)	139.49 ± 19.13	140.00 ± 15.65	0.8992
Total cholesterol, mean ± SD (mmol/L)	4.67 ± 0.96	4.74 ± 1.12	0.7675
Low-density lipoprotein, mean ± SD (mmol/L)	2.89 ± 0.76	2.98 ± 0.88	0.6172
Triglycerides (mmol/L)	1.60 ± 0.64	1.30 ± 0.88	< 0.05
Homocysteine (μmol/L)	13.56 ± 7.01	13.67 ± 5.20	0.9423
CRP (mg/L)	19.35 ± 30.83	6.26 ± 4.80	< 0.05
Fasting plasma glucose, mean ± SD (mmol/L)	6.23 ± 2.78	5.25 ± 0.66	< 0.05
Creatinine, mean ± SD (mmol/L)	79.47 ± 26.34	78.55 ± 17.06	0.8634
Albumin, mean ± SD(g/L)	38.47 ± 26.34	39.39 ± 3.28	0.3491
SBP, mean ± SD (mmHg)	146.17 ± 18.76	135.27 ± 13.87	< 0.05
DBP, mean ± SD (mmHg)	86.40 ± 11.30	86.27 ± 13.87	0.5940
Number of diseased coronary arteries	5.31 ± 2.75	5.12 ± 2.74	0.7687
STEMI/NSTEMI, n (%)			0.2578
STEMI	38(73.07%)	23(74.19%)	
NSTEMI	14(26.93%)	8(25.81%)	
Smoking status, n (%)			0.3072
Yes	32(61.53%)	16(51.61%)	
No	20(38.47%)	15(48.39%)	
Alcohol consumption, n (%)			0.0903
Yes	20(38.47%)	11(35.49%)	
No	32(61.53%)	20(64.51%)	
Hypertension, n (%)			0.3529
Yes	44(84.61%)	27(87.09)	
No	8(15.39%)	4(12.91)	
Diabetes, n (%)			0.4332
Yes	10(19.23%)	8(25.81%)	
No	42(80.77%)	23(74.19%)	

Results

Association between basic participant characteristics, Sac/Val and elevated FGF21 in patients with myocardial infarction

A total of 114 subjects participated in the study, of whom three were excluded due to not meeting the inclusion criteria. The demographic and clinical characteristics of this study population, stratified based on FGF21 levels, are summarized in Table 1. Notably, among patients with MI, those who received Sac/Val therapy exhibited significantly lower levels of triglycerides (1.60 ± 0.64 mmol/L vs. 1.30 ± 0.88 mmol/L; $p < 0.05$), C-reactive protein (CRP) (13.56 ± 7.01 mg/L vs. 6.26 ± 4.80 mg/L; $p < 0.05$), fasting plasma glucose (6.23 ± 2.78 mmol/L vs. 5.25 ± 0.66 mmol/L; $p < 0.05$), and systolic blood pressure (SBP) (146.17 ± 18.76 mmHg vs. 135.27 ± 13.87 mmHg; $p < 0.05$) compared to those who did not receive Sac/Val. No significant socio-demographic differences were observed between the groups.

At various time points after MI surgery - namely, 1 day before, 1 day after, 3 days after, 1 week after, 2 weeks after, and 6 weeks after - serum samples were collected from patients. Postoperatively, patients with MI who received Sac/Val exhibited significantly elevated serum FGF21 levels compared to those with general MI (Fig. 1A). Concurrently, ProBNP and CK-MB levels were notably lower (Fig. 1C and D), while ejection fraction (EF) values were significantly higher (Fig. 1B). However, no significant differences were observed in cTnT and LVDD values between the groups (Fig. 1E and F). Additionally, a statistical analysis of concomitant medication usage revealed no significant differences between the Sac/Val and non-Sac/Val groups. This finding suggests that the observed changes in FGF21 are primarily attributable to Sac/Val treatment, rather than other medications (Supplemental Table 1).

We observed significant changes in FGF21 levels on Day 1 and Day 3. However, due to missing EF data on Day 1, we performed a correlation analysis between FGF21 levels and EF values on Day 3. The results revealed a positive correlation between FGF21 levels and EF ($r = 0.4918$, $p = 0.0171$; Fig. 1G). On the day before surgery, all patients had missing data for LVDD. On postoperative Day 1, data for both LVDD and EF were missing. On Day 3, 9 patients had missing data, and on Day 7, 5 patients had missing data. Missing values were observed due to the surgical procedure. These results offer valuable insights into the potential therapeutic benefits of Sac/Val in the management of MI.

Val, Sac, and Sac/Val all improved left ventricular contractile function, ameliorates cardiac fibrosis, and

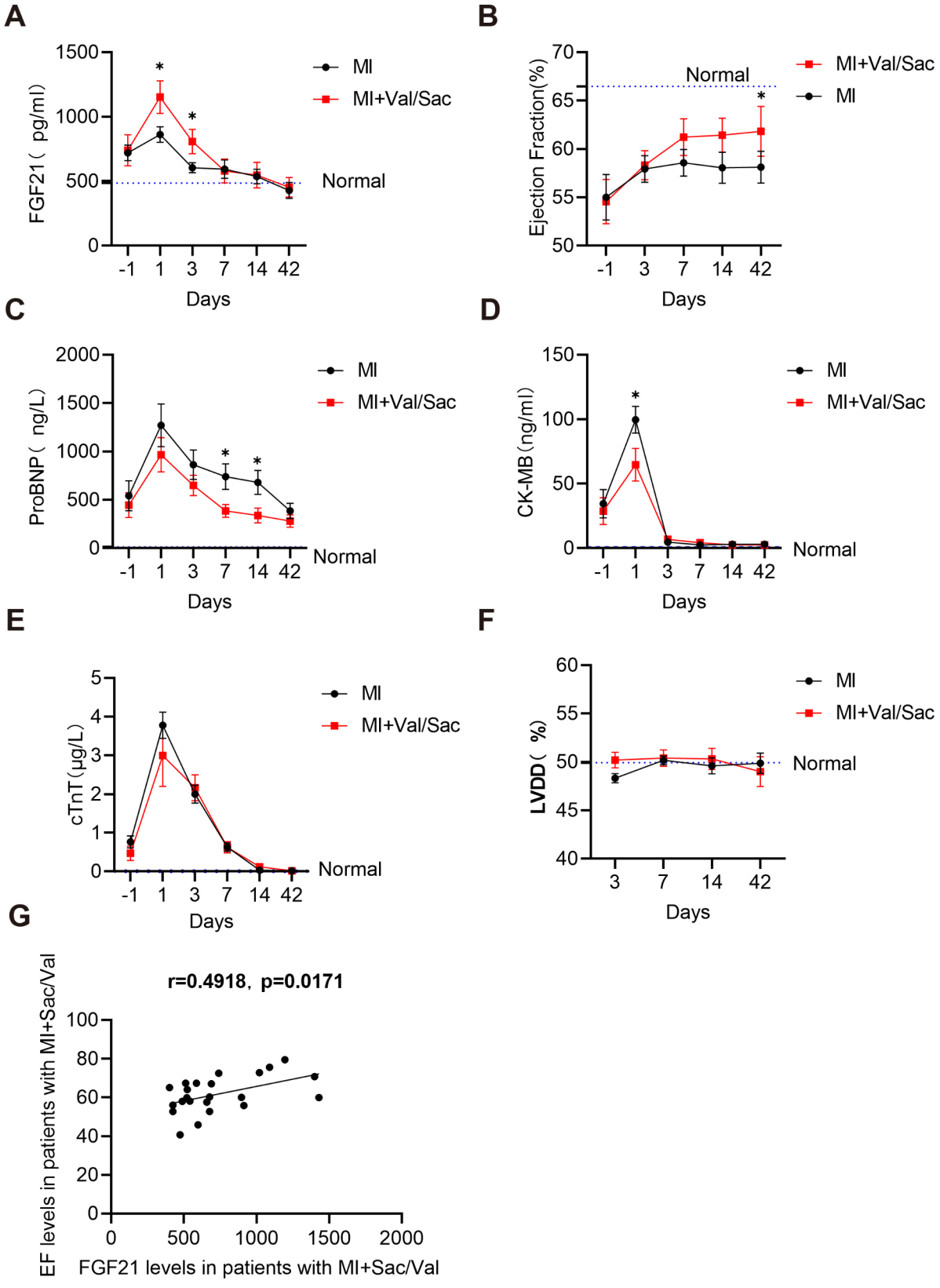

Fig. 1 (See legend on next page.)

(See figure on previous page.)

Fig. 1 The effects of Sac/Val treatment on serum marker levels and cardiac physiological functions in patients with myocardial infarction. The data were obtained from patients with MI taking Sac/Val ($n=31$, as positive controls) and were compared with patients with MI on the same day but not receiving Sac/Val ($n=52$). **A** Serum FGF21 levels; **B** The ejection fraction; **C** Serum ProBNP levels; **D** Serum CK-MB levels; **E** Serum cTnT levels; **F** LVDD levels; **G** Correlation between FGF21 levels and EF levels in patients with MI receiving Sac/Val therapy. The dotted line represents the average value of healthy individuals, which were used as negative controls. ($n=28$). Measurement of FGF21 and EF levels in MI and MI + Sac/Val groups. Panels 1 A, 1 C, 1D, and 1E show data with no missing values for any time point. Panels 1B and 1 F indicate missing values due to the surgical procedure. Specifically, data were missing for all patients on Day 1 post-operation, with 9 patients missing data on Day 3 and 5 patients missing data on Day 7. (A)-(F) * $P<0.05$ indicates MI vs. MI + Sac/Val group within a single day by t-test, all data are expressed as mean ± SEM; (G) p values derived from the Pearson's correlation

reduces reactive oxygen species levels in mice after myocardial infarction.

To validate the efficacy of Sac/Val in elevating heart FGF21 levels in mice with MI, we established a mouse model by ligating the descending branch of the left coronary artery. Subsequently, we compared five distinct treatment regimens: Sham (control), saline (placebo), 26 mg/kg Val, 26 mg/kg Sac, and a combined regimen of 52 mg/kg Sac/Val. There were 12 mice in each group. When the animal model was prepared, 6 mice from each group were used for echocardiography and Western blot analysis, while the remaining 6 mice were used for staining and ELISA. The mice requiring surgery were randomly selected by one researcher and handed over to another researcher responsible for preparing the mouse model, ensuring that the latter was unaware of the group assignments. All subsequent animal models were prepared using this method (Supplemental Fig. 8).

To assess cardiac function, echocardiography was employed (Supplemental Fig. 3). Post-infarction, mice exhibited significant elevations in left ventricular internal diameter during diastole (LVIDd) and left ventricular internal diameter during systole (LVIDs), as well as an increased heart weight to tibia length ratio (HW/TL), accompanied by a significant decline in EF and fractional shortening (FS). Notably, when compared to the MI group, mice treated with Val and Sac exhibited significant reductions in LVIDd, LVIDs, and HW/TL, along with notable improvements in EF and FS. Moreover, the Sac/Val group displayed a more substantial reduction in LVIDd, LVIDs, and HW/TL, as well as a more pronounced increase in EF and FS, compared to the single-dose groups (Fig. 2A and F).

Given the pivotal role of oxidative stress and fibrosis in MI, we investigated whether Sac/Val could modulate reactive oxygen species (ROS) and collagen levels. We evaluated ROS and collagen levels in the hearts of mice from the five groups. Collagen volume fraction (CVF%) was quantified in heart sections using Masson's trichrome staining. MI led to a replacement of myocardial tissue by collagen in WT mice, resulting in a significant increase in CVF% and ROS levels (measured using dihydroethidium (DHE) staining) compared to the Sham group. The Val and Sac groups exhibited significant inhibition of cardiac fibrosis and ROS levels post MI, and the Sac/Val group demonstrated a more pronounced inhibition of both cardiac fibrosis and ROS levels than single dosing (Fig. 2G and I). In all groups, there were six mice in each group, in which three mice hearts were taken from the infarcted area to be used for western blot, and the other three mice were sectioned from the infarcted area to be used for staining such as morphology and immunohistochemistry.

Sac/Val activated the PI3K/AKT/mTOR pathway by up-regulating FGF21 in the liver, heart and circulation

In this study, we investigated the levels of FGF21 in its primary expressing organs and discovered a notable upregulation of FGF21 expression in the liver, heart, and circulation of mice administered with Val and Sac. Mice were blooded on day 14 of the model and assayed for FGF21. However, no significant alterations were observed in adipose tissue. Remarkably, the combined therapy of Sac/Val resulted in significantly higher expressions of FGF21 compared to the single-agent administration (Fig. 3A and D).

We have demonstrated that Sac/Val could upregulate FGF21, which aids in mitigating MI. However, the specific mechanism underlying the role of FGF21 in Sac/Val-mediated cardio-protection remains elusive. Our analysis revealed significantly higher expression ratios of phosphorylated PI3K/PI3K, p-AKT/AKT, and p-mTOR/mTOR proteins in the hearts of mice treated with Val or Sac compared to MI group. Furthermore, these ratios were even more elevated in the Sac/Val combination group compared to single-agent treatment. Additionally, we observed a significant downregulation of HIF-1α, α-SMA, and collagen-I protein expression in the Val and Sac groups relative to the MI group, with an even more profound decrease observed in the Sac/Val group (Fig. 3E).

To further elucidate the mechanism, we utilized H9C2 cells and blocked PI3K activity using a specific inhibitor. This approach abolished the activation of the PI3K/AKT/mTOR signaling axis induced by Sac/Val (Supplemental Fig. 1A-1 C).

Collectively, our findings convincingly demonstrate that Sac/Val positively modulates and augments hepatic and circulating FGF21 levels, concomitantly activating the intricate FGFR1/PI3K/AKT/mTOR signaling cascade within the heart, thus providing significant cardio-protection.

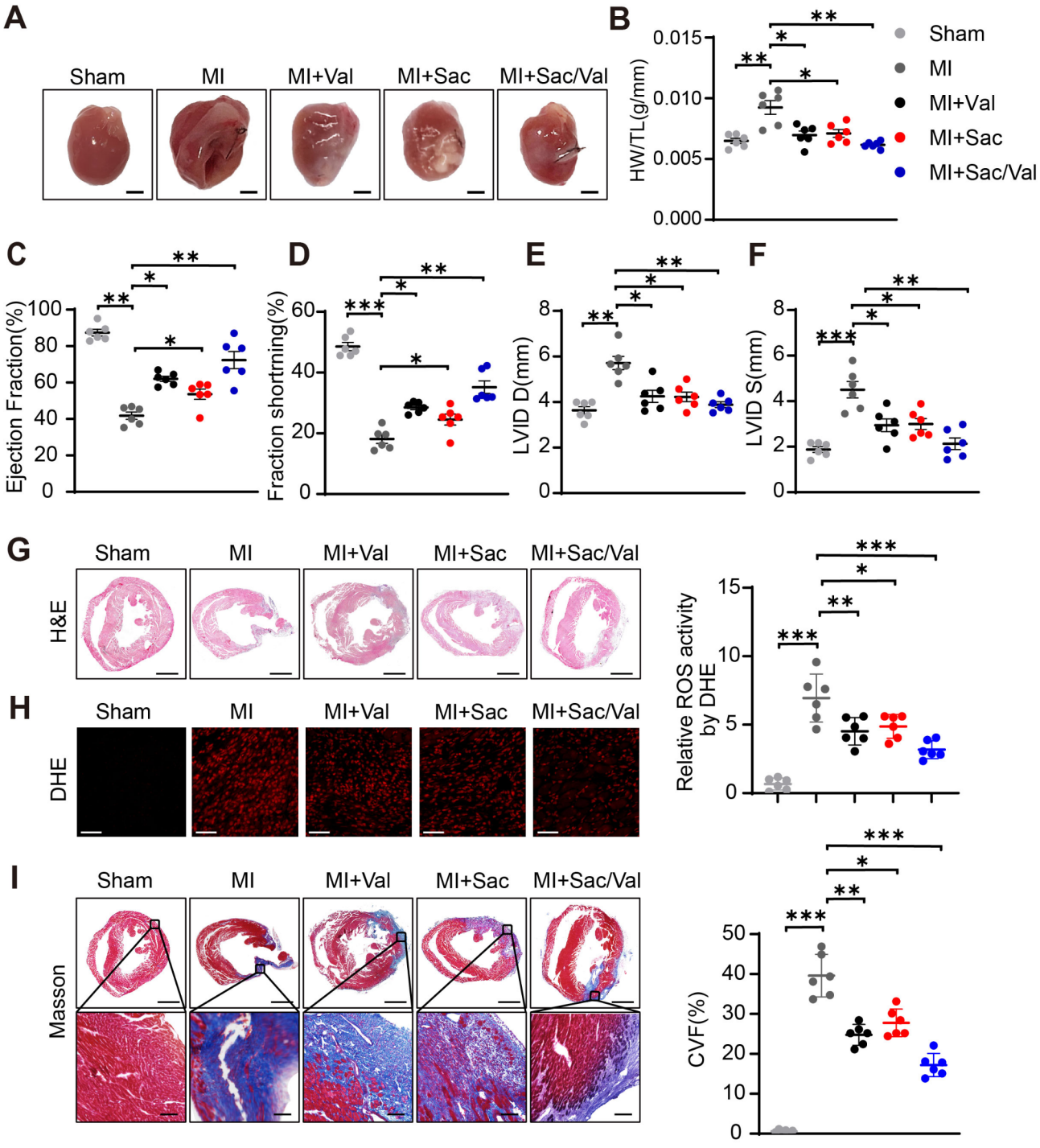

Fig. 2 Therapeutic Effects of Sac/Val and Its Constituents on Cardiac Function and Pathology Post-Myocardial Infarction in Mice. **A** Representative macroscopic photographs of hearts (scale bar, 2 mm); **B** HW (grams) to tibial length (TL; millimeters) ratio; **C** Left ventricular ejection fraction (EF); **D** Left ventricular short axis (FS); **E** Left ventricular end-diastolic diameter (LVIDD); **F** Left ventricular systolic diameter systole (LVIDS); **G** Hematoxylin-eosin (HE)–stained sections of hearts. Above: original magnification ×4(scale bar, 2 mm); **H** Measurement of ROS levels in the hearts. Dihydroethidium staining was performed to assess cellular ROS (Scale bars, 50 mm); **I** The myocardial infarct size was measured with Masson's trichrome staining. The images show that the fibrosis marker was stained in blue, whereas cardiac muscle fibers were in red and nuclei in dark brown. Above: original magnification ×4(scale bar, 2 mm); below original magnification ×20 (Scale bar, 100 μm). Data are expressed as mean ± SEM; $n = 6$ per group, three independent experiments were repeated; to determine statistical differences between two groups, one-way ANOVA along with Tukey's post hoc test were used to compare difference among groups.; * $P < 0.05$, ** $P < 0.01$, *** $P < 0.001$

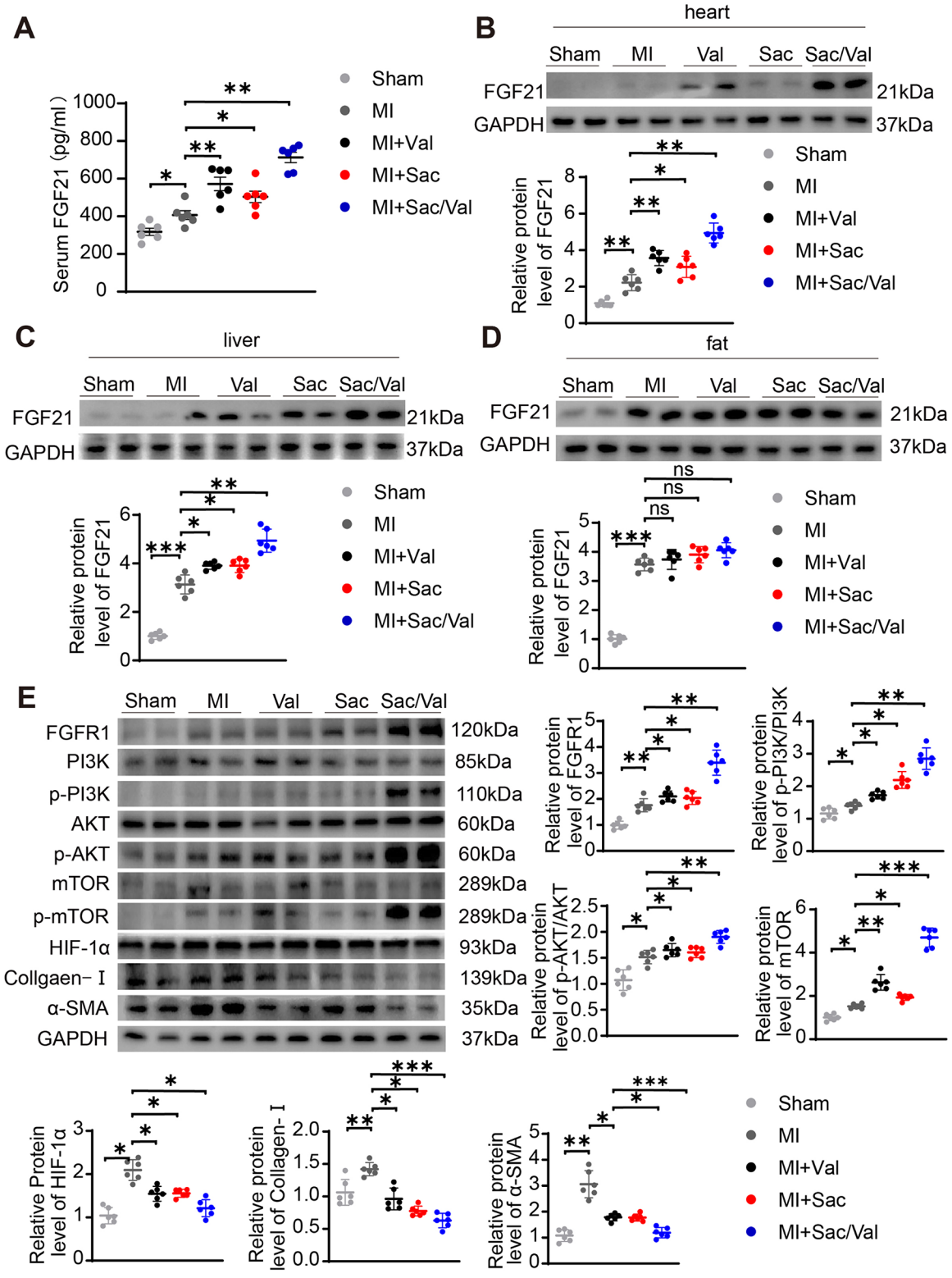

Fig. 3 Elevation of FGF21 Expression and Activation of PI3K/AKT/mTOR Signaling Pathway in the Liver, Heart, and Circulation Following Sac/Val Administration. **A** Serum FGF21 levels; **B** Protein of FGF21 in the heart, **C** liver, and **D** fat of Sham, MI, Val, Sac, and Sac/Val mice were examined by Western blotting; **E** Protein levels of FGFR1, PI3K/t-PI3K ratio, p-AKT/t-AKT ratio, p-mTOR/mTOR ratio, HIF-1α, collagen-I, and α-SMA in the heart of mice were examined by Western blotting. Data are expressed as mean ± SEM; $n = 6$ per group, three independent experiments were repeated; to determine statistical differences between two groups, one-way ANOVA along with Tukey's post hoc test were used to compare difference among groups.; * $P < 0.05$, ** $P < 0.01$, *** $P < 0.001$

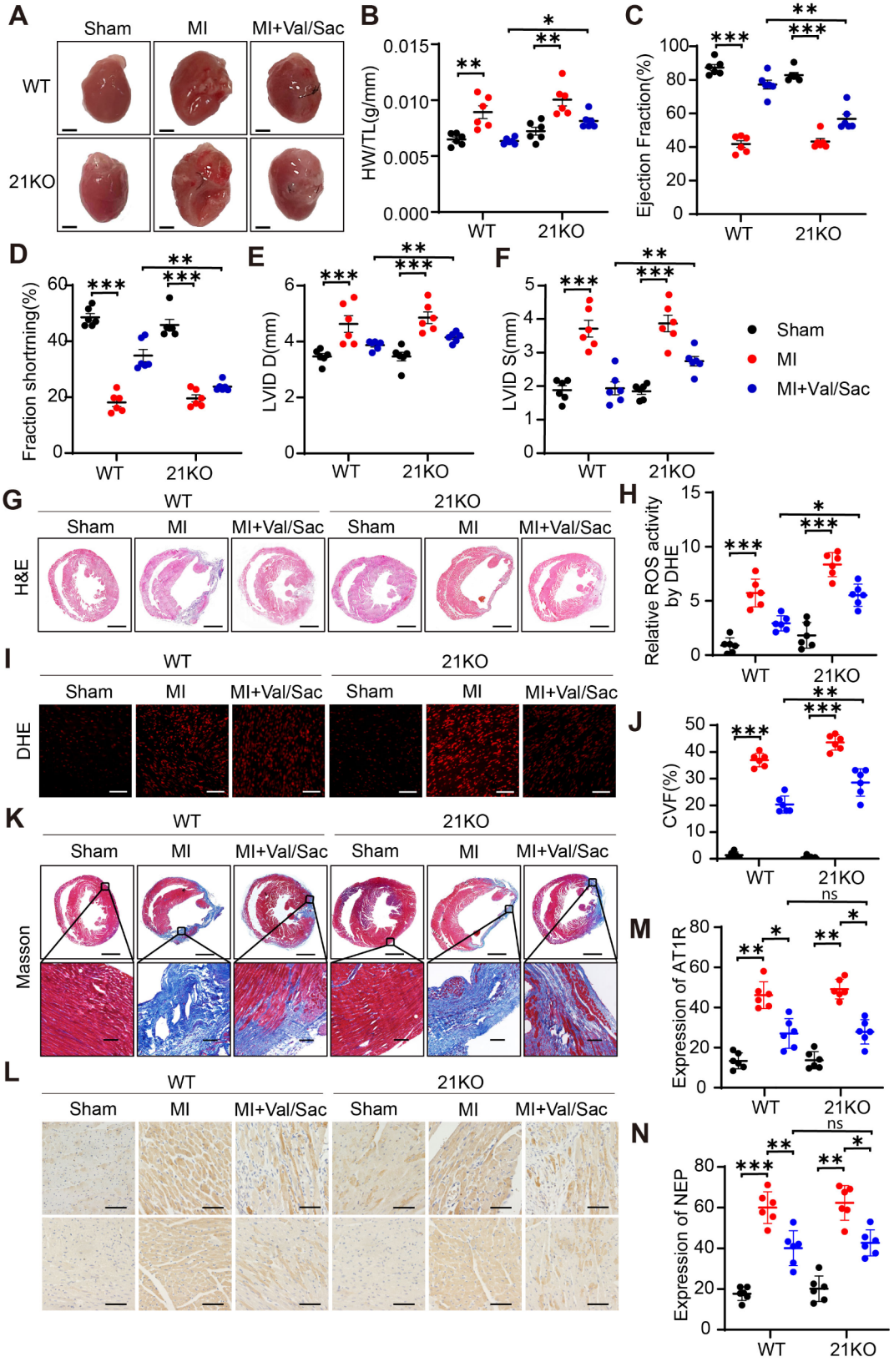

Fig. 4 (See legend on next page.)

(See figure on previous page.)

Fig. 4 FGF21 gene knockout attenuates the beneficial effects of Sac/Val on left ventricular function, reduction of myocardial fibrosis, and decrease in reactive oxygen species in acute myocardial infarction, but does not affect its inhibitory effects on atrial natriuretic peptide and angiotensin II type 1 receptor signaling pathway. **A** Representative macroscopic photographs of hearts (scale bar, 2 mm); **B** HW (grams) to tibial length (TL; millimeters) ratio; **C** Left ventricular ejection fraction (EF); **D** Left ventricular short axis (FS); **E** Left ventricular end-diastolic diameter (LVIDD); **F** Left ventricular systolic diameter systole (LVIDS); **G** Hematoxylin-eosin (HE)–stained sections of hearts. Above: original magnification ×4(scale bar, 2 mm); **H** Measurement of ROS levels in the hearts; (I) Dihydroethidium staining was performed to assess cellular ROS (Scale bars, 50 mm); **J** and **K** The myocardial infarct size was measured with Masson's trichrome staining; **L**-**N** Immunohistochemical staining of heart sections for AT1R and NEP, scale bar: 100 μm. Data are expressed as mean ± SEM; $n = 6$ per group, three independent experiments were repeated; to determine statistical differences between two groups, one-way ANOVA along with Tukey's post hoc test were used to compare difference among groups.; * $P < 0.05$, ** $P < 0.01$, *** $P < 0.001$

The effects of Sac/Val on improving left ventricular systolic function, relieving cardiac fibrosis, and reducing reactive oxygen species levels were partially inhibited and partially restored by FGF21 knockdown and backfill.

To further confirm whether FGF21 mediates the protective effect of Sac/Val against MI injury, we conducted two rounds of experiments using a mouse MI model established by ligation of the left anterior descending coronary artery. The animals were grouped as follows in the first round of experiments: Sham controls, MI + PBS, MI + Sac/Val WT mice, FGF21KO Sham controls, FGF21KO MI + PBS, and MI + Sac/Val FGF21KO mice. Additionally, we included Sham and FGF21KO mice administered with 52 mg/kg of Sac/Val and AAV-GFP or AAV-FGF21 vectors (Supplemental Fig. 2A-2D). To assess cardiac function, echocardiography was employed (Supplemental Figs. 3 and 4). Our results indicated that Sac/Val can significantly improve left ventricular systolic function, reduce cardiac fibrosis, and lower ROS levels in wild-type MI mice, but these effects are significantly attenuated in FGF21KO MI mice (Fig. 4A and M).Next we calculated the effects size in WT and FGF21KO mice administered and unadministered, in WT mice, the effects size of HW/TL, EF, FS, LVIDd, LVIDs, ROS levels and fibrosis levels were 0.78704, 0.95105, 0.87916, 0.58267, 0.85328, 0.80315, 0.94539, while in FGF21KO mice were 0.65811, 0.75675, 0.64629, 0.6782, 0.7522, 0.79904, 0.87415, respectively, and the effects sizes of other WTs were greater than those of FGF21KO, except for LVIDd. Therefore, we concluded that the beneficial effect of Sac/Val on myocardial infarction in FGF21 KO mice was significantly attenuated.

In a subsequent experimental round, we observed significant restoration of left ventricular systolic function, cardiac fibrosis, and reductions in ROS levels in the FGF21KO 52 mg/kg Sac/Val AAV-FGF21 group compared to the FGF21KO 52 mg/kg Sac/Val AAV-GFP group (Fig. 5A and I). Intriguingly, when we investigated the endogenous pathways of valsartan and Sacubitril, we discovered that the expression of AT1R and NEP remained largely unchanged in both FGF21knockout and replenished MI models (Figs. 4L and N and 5J). These results indicate that FGF21 represents a novel downstream signal of Sac/Val in MI.

Sac/Val mediates regulation of FGF21 through PPARs

Next, we aimed to elucidate the mechanism underlying Sac/Val's regulation of FGF21. Initially, we investigated the interaction between Sac/Val and PPARs using molecular docking. The lowest energies for Sac-PPARα and Val-PPARα interaction were −7.7 kcal/mol and −7.3 kcal/mol respectively (Fig. 6A). Similarly, for Sac-PPARγ and Val-PPARγ interaction, the lowest binding energies were −8.3 kcal/mol and −8.2 kcal/mol respectively (Supplemental Fig. 7A).

To validate valsartan and sacubitril as bona fide PPARα ligands and quantify their binding affinity, we employed a surface plasmon resonance (SPR)-based assay. In PPARα, fenofibrate served as a positive control, exhibiting a thermodynamic dissociation constant (KD) of 1.079×10^{-5} M, indicating a stable complex formation with PPARα. Valsartan and sacubitril displayed a similar trend, albeit with significantly lower affinity for PPARα, as evidenced by their KD values of 1.209×10^{-4} M and 2.04×10^{-4} M, respectively (Fig. 6B and D). In AML-12 cells, we used a concentration gradient to determine the optimal dose concentrations of the PPARα-specific inhibitors GW6471 and Sac/Val (Supplemental Fig. 5B), and next we observed that GW6471 significantly mitigated the Sac/Val-induced upregulation of FGF21 (Fig. 6E).

For PPARγ, rosiglitazone served as the positive control, exhibiting a KD of 8.485×10^{-7} M, indicating a stable complex formation. However, only sacubitril displayed detectable binding to PPARγ with a KD of 1.579×10^{-5} M, while valsartan showed no significant binding (Supplemental Fig. 7B-6E). Subsequently, we incubated H9C2 cells under hypoxic conditions of 5% O_2 and employed a concentration gradient to identify the optimal dosing concentrations for the PPARγ-specific inhibitor GW9662 and Sac/Val (Supplemental Fig. 5A). Our results revealed that GW9662 effectively blocked PPARγ and significantly abrogated the Sac/Val-induced upregulation of FGF21 (Supplemental Fig. 7E).

To further formalize whether PPARs mediates Sac/Val modulation of FGF21 to ameliorate myocardial infarction in mice. We prepared five groups of models by feeding Sac/Val and administering inhibitors of PPARα and PPARγ. The animals were grouped as follows: sham controls, MI + PBS, MI + Sac/Val WT mice, MI + Sac/Val WT + GW9662 mice, and MI + Sac/Val WT + GW6471

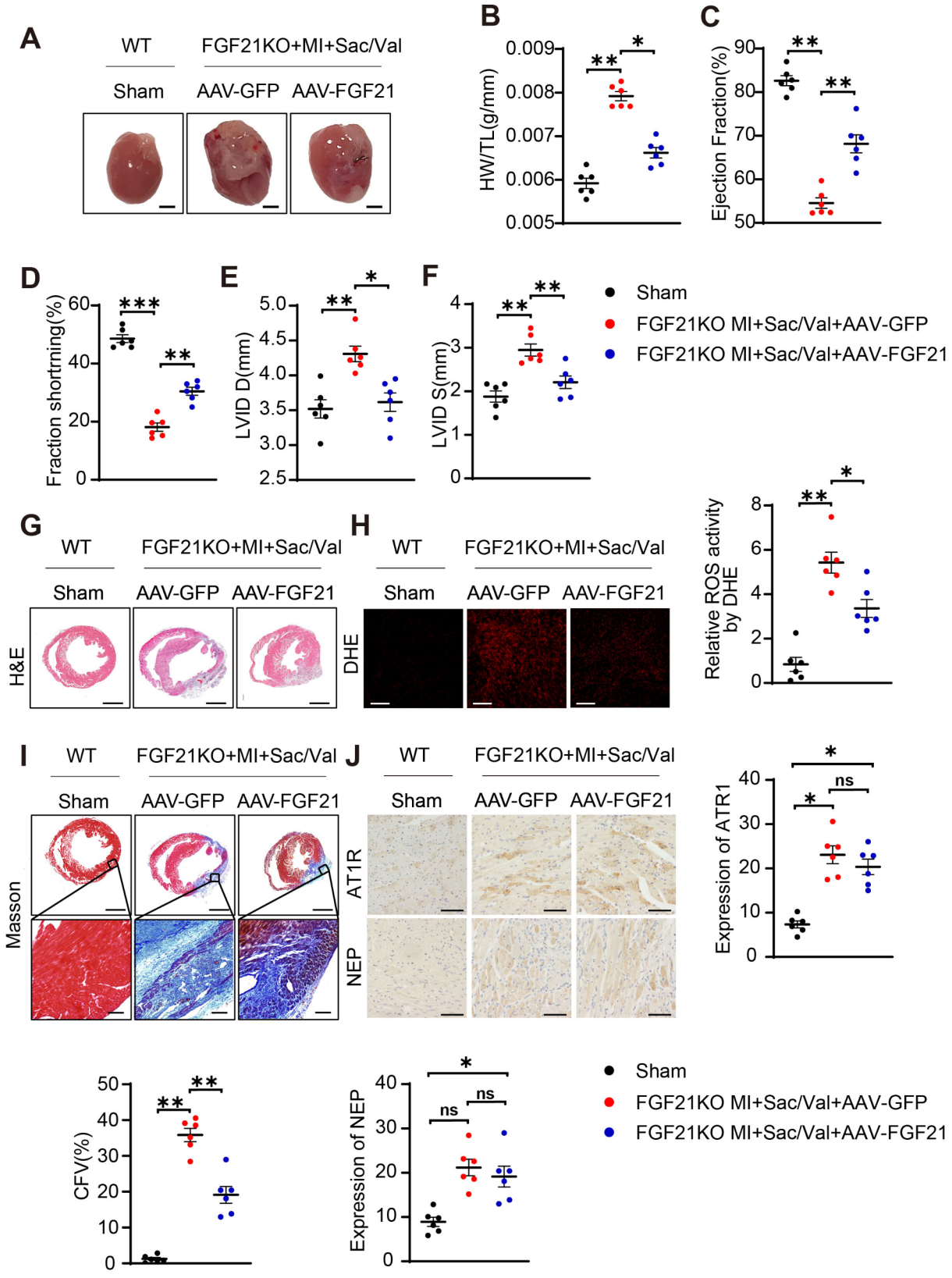

Fig. 5 (See legend on next page.)

(See figure on previous page.)

Fig. 5 The administration of Sac/Val significantly enhances left ventricular systolic function, mitigates cardiac fibrosis, and diminishes reactive oxygen species levels in myocardial infarcted mice following the restoration of FGF21 expression, without exerting any notable impact on ANP and AT1R signaling pathway. **A** Representative macroscopic photographs of hearts (scale bar, 2 mm); **B** HW (grams) to tibial length (TL; millimeters) ratio; **C** Left ventricular ejection fraction (EF); **D** Left ventricular short axis (FS); **E** Left ventricular end-diastolic diameter (LVIDD); **F** Left ventricular systolic diameter systole (LVIDS); **G** Hematoxylin-eosin (HE)–stained sections of hearts. Above: original magnification ×4(scale bar, 2 mm); **H** Measurement of ROS levels in the hearts. Dihydroethidium staining was performed to assess cellular ROS (Scale bars, 50 mm); **I** The myocardial infarct size was measured with Masson's trichrome staining; **J** Immunohistochemical staining of heart sections for AT1R and NEP, scale bar: 100 μm. Data are expressed as mean ± SEM; $n = 6$ per group, three independent experiments were repeated; to determine statistical differences between two groups, one-way ANOVA along with Tukey's post hoc test were used to compare difference among groups.; * $P < 0.05$, ** $P < 0.01$, *** $P < 0.001$

mice. To assess cardiac function, echocardiography was employed (Supplemental Fig. 5). Our results showed that GW9662 and GW6471 significantly partially blocked Sac/Val improved LV systolic function, cardiac fibrosis, and ROS levels in wild-type MI mice (Fig. 7A and I). We next examined the expression of PPARγ and FGF21 in the hearts of mice that had been administered GW9662, and we found that Sac/Val significantly upregulated PPARγ in the hearts of mice with myocardial infarction, whereas administration of GW9662 significantly downregulated PPARγ in the hearts of mice with myocardial infarction and blocked the up-regulatory effect of Sac/Val on FGF21. Similarly, Sac/Val significantly upregulated PPARα in the livers of mice with myocardial infarction, whereas administration of GW6471 significantly downregulated PPARα in the livers of mice with myocardial infarction and blocked the up-regulatory effect of Sac/Val on FGF21 (Fig. 7J and K).

In summary, these findings indicate that the beneficial effects of Sac/Val in MI mice are partially mediated through the modulation of PPARs.

Discussion

In the PARADISE-MI trial, the risk of the primary endpoint events (cardiovascular death, first heart failure hospitalization, and outpatient progression to heart failure) was reduced by 10% in the ARNI group compared with the ramipril group. Thus Sac/Val remains an excellent drug for improving myocardial infarction [3]. Despite the clinical proficiency demonstrated by Sac/Val, a comprehensive elucidation of its underlying molecular mechanisms at the cellular level remains elusive. FGF21, initially identified as a modulator of glucolipid metabolism and insulin secretion, has garnered increasing attention in subsequent clinical studies. These investigations have revealed that FGF21 binds to FGFR1 in the heart, exhibiting autocrine or paracrine properties, and emerges as a promising biomarker for predicting cardiovascular diseases, such as AMI and coronary artery disease. Moreover, FGF21 exhibits potential therapeutic value in the prevention and rehabilitation of cardiovascular pathologies [7, 21, 22]. The objective of the present study was to delve into the potential of Sac/Val to function as an agonist of FGF21, thereby mitigating the severity of MI.

Initially, we recruited a cohort of patients diagnosed with MI from our clinical setting. Our findings revealed that Sac/Val administration resulted in a marked enhancement of ejection fraction in these patients, aligning with previous research and demonstrating improvements in several cardiac function indices. Notably, we observed a significant elevation in circulating FGF21 expression among patients with MI receiving Sac/Val compared to those not receiving this treatment. Furthermore, the FGF21 expression exhibited a positive correlation with EF levels in patients with Sac/Val. These results in patients with MI were in line with our initial hypotheses.

To further substantiate our observations, we conducted subsequent experiments using a mouse model. Based on extensive literature reports indicating that a dosage of 52 mg/kg/day is commonly employed in mice, we selected this dose for our study, as it has been validated to be both safe and reliable. Although this dosage may partially differ from that used in clinical practice, it provides a robust foundation for preclinical evaluation. As anticipated, Sac/Val demonstrated significantly greater protective effects against the decline in cardiac function in the ligated left anterior descending artery (LAD)-induced infarct mouse model compared to equimolar low-dose Val and Sac administered individually. This finding aligns with previous reports, thereby reinforcing the validity and credibility of our research. Following MI, the liver is a major source of FGF21 production, while the heart itself also exhibits elevated FGF21 levels post-cardiac injury. The endocrine function of liver-derived FGF21, coupled with the autocrine production of FGF21 by the heart, contributes to cardio-protection [11, 23]. Additionally, adipose tissue serves as a significant source of FGF21 secretion. In our study, we evaluated the expression of FGF21 in the heart, liver, adipose tissue, and systemic circulation. As anticipated, both Val and Sac, administered as single doses, led to significant elevations in FGF21 expression in the heart, liver, and circulation, compared to equimolar low-dose treatments of Val and Sac. However, we did not observe notable increases in FGF21 expression in adipose tissue. These findings indicate that Sac/Val upregulates FGF21 expression in the liver, heart, and circulation.

In the heart, FGF21 exerts its beneficial effects by alleviating cardiac impairment and fibrosis through

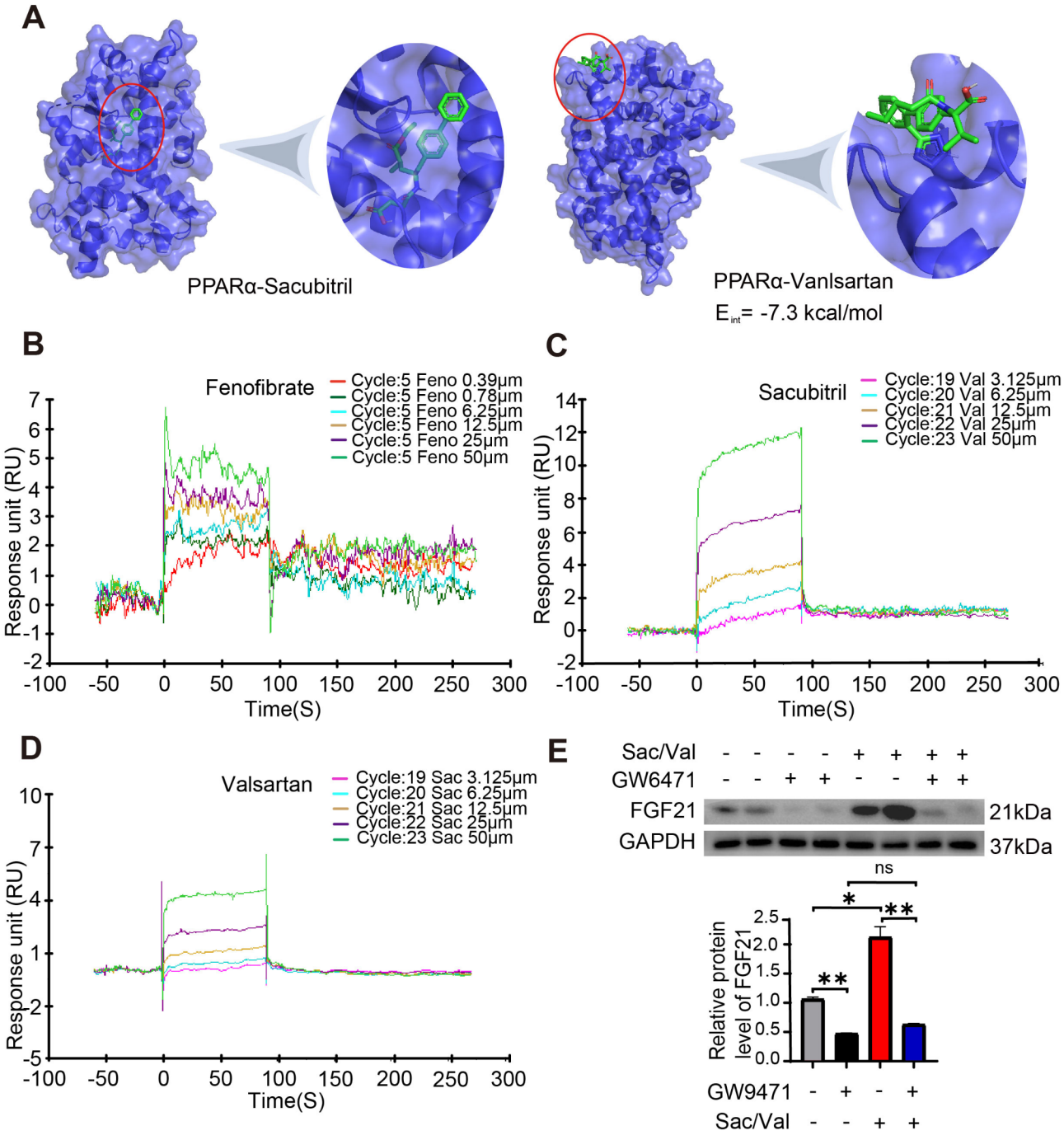

Fig. 6 Sac/Val-Mediated Upregulation of FGF21 in the Liver via PPARα. **A** Molecular modeling of the interaction between Valsartan, Sacubitril, and PPARα; Sensorgrams obtained injecting different concentrations of **B** Fenofibrate, **C** sacubitril and **D** valsartan on immobilized PPARα; **E** AML-12 Cells were untreated or treated with GW6471 (10μM) for 12 h, then incubated in the presence or absence of Sac/Val (20μM), FGF21 were detected by Western blotting. Data are expressed as mean ± SEM; three independent experiments were repeated; to determine statistical differences between two groups, one-way analysis of ANOVA was employed; * $P < 0.05$, ** $P < 0.01$, *** $P < 0.001$

the inhibition of endoplasmic reticulum stress-induced apoptosis, mediated by the activation of the FGFR1/PI3K/AKT signaling pathway, and ameliorating oxidative stress by modulating the Sirt3/MnSOD pathway [24–26]. Furthermore, mTOR plays a crucial role in protecting the heart from ischemic injury. We subsequently investigated the expression of downstream signaling components in the mouse heart. In accordance with our initial supposition, the Sac/Val complex significantly upregulated the expression of not only FGF21 but also the crucial

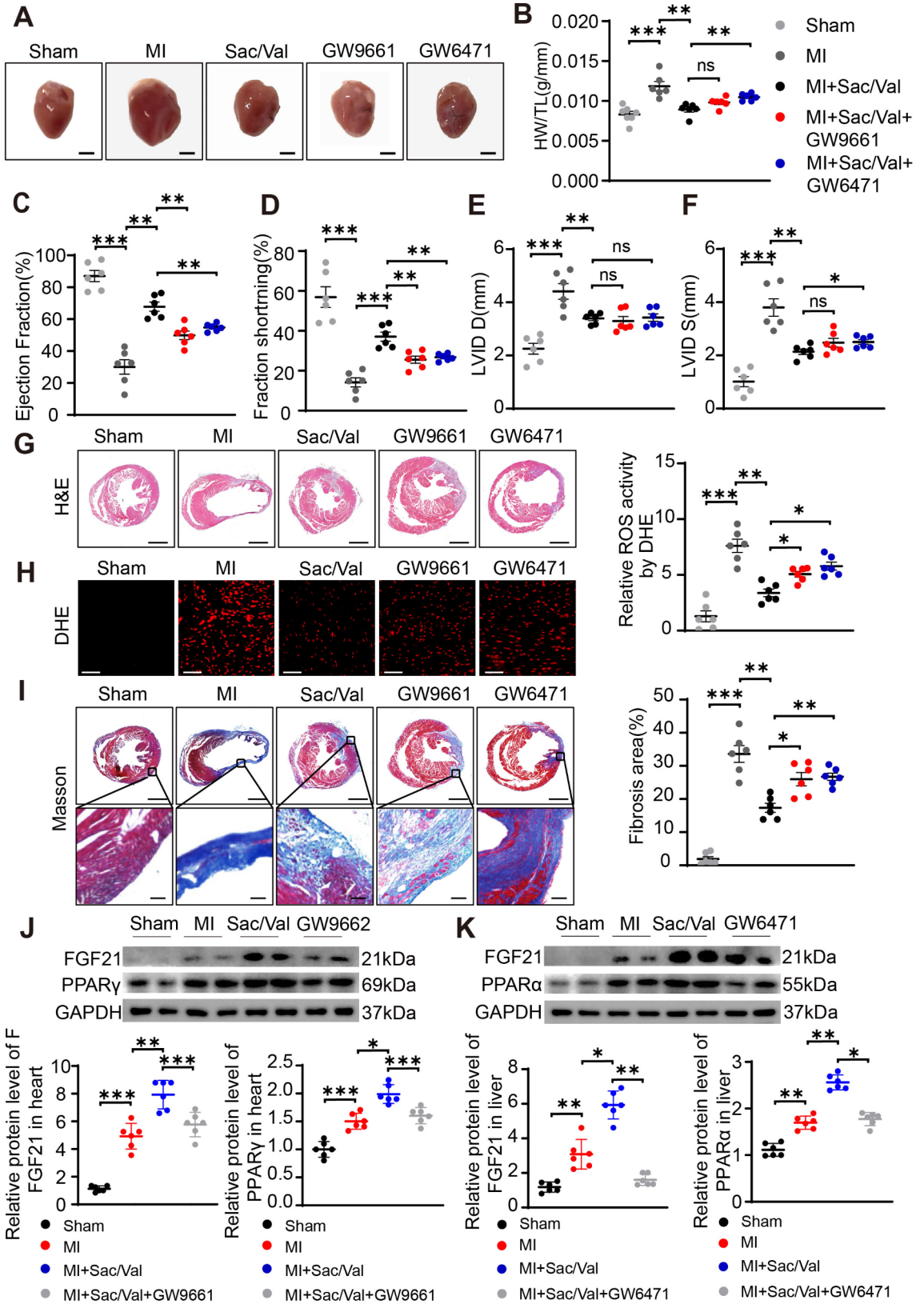

Fig. 7 (See legend on next page.)

(See figure on previous page.)

Fig. 7 PPARα and PPARγ inhibition partially blocked the up-regulatory effect of Sac/Val on FGF21 and the ameliorative effect on myocardial infarction mice. **A** Representative macroscopic photographs of hearts (scale bar, 2 mm); **B** HW (grams) to tibial length (TL; millimeters) ratio; **C** Left ventricular ejection fraction (EF); **D** Left ventricular short axis (FS); **E** Left ventricular end-diastolic diameter (LVIDD); **F** Left ventricular systolic diameter systole (LVIDS); **G** Hematoxylin-eosin (HE)–stained sections of hearts. Above: original magnification ×4(scale bar, 2 mm); (H) Measurement of ROS levels in the hearts. Dihydroethidium staining was performed to assess cellular ROS (Scale bars, 50 mm); **I** The myocardial infarct size was measured with Masson's trichrome staining. The images show that the fibrosis marker was stained in blue, whereas cardiac muscle fibers were in red and nuclei in dark brown. Above: original magnification ×4(scale bar, 2 mm); below original magnification ×20 (Scale bar, 100 μm); **J** Protein of FGF21 and PPARγ in the heart were examined by Western blotting; **K** Protein of FGF21 and PPARα in the liver were examined by Western blotting. Data are expressed as mean ± SEM; $n = 6$ per group, three independent experiments were repeated; to determine statistical differences between two groups, one-way analysis of ANOVA was employed; * $P < 0.05$, ** $P < 0.01$, *** $P < 0.001$

components that comprise its downstream signaling pathway, further corroborating our scientific prediction. Notably, when we blocked PI3K, we observed that Sac/Val failed to activate the PI3K/AKT/mTOR signaling axis, further validating the critical role of this pathway in mediating the cardioprotective effects of Sac/Val.

Subsequently, we developed a mouse model of MI using FGF21KO mice to further investigate the role of FGF21. Our findings revealed that upon FGF21 knockdown, cardiac functions, fibrosis, and oxidative stress were exacerbated in mice with MI, corroborating previous research. Furthermore, when FGF21 was genetically ablated, it partially hindered the beneficial effects of Sac/Val on MI in these mice. However, when FGF21 was replenished, the positive response to Sac/Val treatment was reinstated. Notably, we observed that the expression of the original target of Sac/Val action was not significantly altered by FGF21 knockdown or replenishment. These results suggest that FGF21 represents a novel target, independent of the primary target, for Sac/Val to attenuate MI.

Activation of peroxisome proliferator-activated receptors (PPARs), comprising PPARα, PPARβ/δ, and PPARγ, has been extensively documented to exhibit salutary effects in cardiovascular diseases, including atherosclerosis and MI [21–23]. Specifically, in the liver, FGF21 serves as a critical mediator of PPARα's pleiotropic functions. FGF21 is directly induced by PPARα in hepatic tissue, whereas in the heart, PPARγ has been shown to enhance left ventricular remodeling and cardiac function post-MI. Numerous studies have highlighted FGF21 as a pivotal mediator of the physiological and pharmacological actions of PPARγ in this context [15–17].

To elucidate the potential interactions between Sac/Val and PPARs, we performed molecular docking studies with PPARα and PPARγ, revealing stable docking configurations, suggestive of Sac/Val's potential as an agonist for both receptors. Subsequently, in surface plasmon resonance (SPR) experiments, we observed robust binding of Sac/Val to PPARα, while the binding to PPARγ was comparatively less robust. Subsequently, in vitro experiments utilizing AML-12 cells and H9C2 cells revealed that the upregulation of FGF21 by Sac/Val was attenuated upon the administration of inhibitors targeting PPARα and PPARγ, respectively. Next, we further verified the effect of PPARs on the modulation of FGF21 by Sac/Val in animals. By administering inhibitors of PPARs, we found that the upregulation of FGF21 by Sac/Val was partially blocked, and the ameliorative effect of Sac/Val on mice with myocardial infarction was also partially blocked.

Interestingly, we found that the ameliorative effect of Sac/Val on LVID D was not blocked after administration of GW9662 versus GW6471, whereas GW6471 blocked the ameliorative effect of Sac/Val on LVID S, whereas GW9662 did not. We therefore conclude that the liver is the predominant source of FGF21 and that the liver contributes more than the heart to the improvement of myocardial infarction. Collectively, our experimental data suggests that PPARs play a pivotal mediating role in the liver, a supportive yet partial role in the heart, and exhibit a multi-organ interplay via the circulatory system. In conclusion, Sac/Val exerts its regulatory effects on FGF21 upregulation through the mediation of PPARs.

Since the groundbreaking discovery of FGF21 in 2000, our comprehension of its biological and pathophysiological roles has undergone significant advancements. The natural, mature human FGF21 hormone comprises 179 amino acid residues, significantly exceeding the lengths of intestinal or pancreatic hormones such as GLP-1 (30 or 31 amino acids), GIP (42 amino acids), glucagon (29 amino acids), and GLP-2 (33 amino acids). This extended length poses challenges in the development of FGF21 as a therapeutic agent, as well as limits its clinical application due to in vitro instability and a short half-life in vivo [27, 28].

In contrast, Sac/Val, a chemically synthesized agent, offers several advantages, including high stability, ease of transportation, and a simplified administration method. In this study, we discovered for the first time that Sac/Val functions as a potential FGF21 agonist. Specifically, Sac/Val upregulates FGF21 levels through partial activation of peroxisome proliferator-activated receptors, thereby mitigating fibrosis and oxidative stress in MI. Our findings strengthen the evidence for the cross-protective effects of FGF21 between the liver and heart.

In conclusion, Sac/Val ameliorates myocardial infarction partly through FGF21, a novel agonist of FGF21, and also further clarifies the mechanism of FGF21 in

myocardial infarction. This study provides theoretical support and experimental basis for the development of new strategies for the treatment of myocardial infarction, and provides a basis for the development of new indications for Sac/Val.

Supplementary Information

The online version contains supplementary material available at https://doi.org/10.1186/s12933-025-02627-6 .

Additional file1: Supplemental Fig. 1. Activation of the PI3K/AKT/mTOR axis by Sac/Val was blocked after the PI3K blockade. (A)-(C) Protein levels of PI3K/t-PI3K ratio and p-AKT/t-AKT ratio in the H9C2 cells were examined by Western blotting. Data are expressed as mean±SEM; three independent experiments were repeated; to determine statistical differences between two groups, one-way analysis of ANOVA was employed; * $P < 0.05$, ** $P < 0.01$, *** $P < 0.001$.Supplemental Fig. 2. AAV-FGF21 onset of action (A) Mouse blood sampling timeline; (B)-(D) Serum FGF21 levels. Data are expressed as mean ± SEM; to determine statistical differences between two groups, one-way analysis of ANOVA was employed; * $P < 0.05$, ** $P < 0.01$, *** $P < 0.001$. Supplemental Fig. 3. Representative photographs of M-mode echocardiography of left ventricle (LV). Representative photograph of left ventricular M-mode echocardiogram during Sac/Val administration. Supplemental Fig. 4. Representative photographs of M-mode echocardiography of left ventricle (LV). (A) Representative Photographs of Left Ventricular M-Mode Echocardiography in FGF21 Knockout; (B) Representative Photograph of Left Ventricular M-Mode Echocardiogram in FGF21 Backfill. Supplemental Fig. 5. Representative photographs of M-mode echocardiography of left ventricle (LV). Representative photograph of left ventricular M-mode echocardiogram during Sac/Val administration. Supplemental Fig. 6. The setting of the concentration gradient of drug delivery. (A)-(B) Protein levels of PPARα in the AML-12 cells and PPARγ in the H9C2 cells were examined by Western blotting. Data are expressed as mean ± SEM; three independent experiments were repeated; to determine statistical differences between two groups, one-way analysis of ANOVA was employed; * $P < 0.05$, ** $P < 0.01$, *** $P < 0.001$. Supplemental Fig. 7. Sac/Val mediated upregulation of FGF21 in heart via PPARγ. (A) Molecular modeling of the interaction between Valsartan, Sacubitril, and PPARγ; Sensorgrams obtained injecting different concentrations of (D) rosiglitazone, (C) sacubitril and (D) valsartan on immobilized PPARα; (E) H9C2 Cells were untreated or treated with GW9662(10μM) for 12 h, incubated for 12 h in the presence or absence of Sac/Val (20 μM) while incubating hypoxically. FGF21 were detected by Western blotting. Data are expressed as mean ± SEM; three independent experiments were repeated; to determine statistical differences between two groups, one-way analysis of ANOVA was employed; * $P < 0.05$, ** $P < 0.01$, *** $P < 0.001$. Supplemental Fig. 8. Experimental Design and Animal Grouping. The experimental design and grouping of mice used to investigate the effects of Sac/Val on myocardial infarction and its mechanistic link to FGF21. Four rounds of experiments were conducted, involving wild-type (WT) and FGF21 knockout (KO) mice, with different treatment groups. The experiments included echocardiography, Western blot analysis, staining, and ELISA to assess cardiac function, fibrosis, and oxidative stress. Supplemental Fig. 9. Schematic diagram of the mechanism by which Sac/Val ameliorates fibrosis and oxidative stress in mice with myocardial infarction by regulating FGF21 through PPARs. Sac/Val ameliorated fibrosis and oxidative stress in mice with MI by regulating PPARs in the liver and heart, causing cardiac autocrine or blood circulation upregulation of FGF21, and through the FGF21/PI3K/AKT/mTOR axis. The gray box shows the classical target of action of Sac/Val, and FGF21 is a new target independent of the original target. Supplemental Table 1. Comparison of concomitant medication usage rates between patients receiving Sac/Val and those not receiving Sac/Val.

Acknowledgements
Nothing to declare.

Author contributions
Wei Wenjuan: conceptualization, methodology, and funding acquisition. Xu Guangsen: methodology, validation, formal analysis, data curation and wrote the first draft of the manuscript. Gao Jiaer, Wang Guiyun, Wang Ye, Li Caiyan, Zheng Junwei, Lu Huiying and Lu Yunyan: methodology, validation, and performed statistical analysis and formal analysis. Wang Kun: molecular docking. Xu Hongtao: funding acquisition. Wang Cong: Conceptualization, Resources, Investigation, Project administration; Pan Xuebo: conceptualization, resources, writing-review & editing, supervision, project administration, funding acquisition.

Funding
This work was funded by Natural Science Foundation of Zhejiang Province, Grant (LR20H310001); Zhejiang Provincial Medical and Health Technology Plan (2023KY226); Zhejiang Province Medical and Health Research Program (2021KY1244).

Aavailability of data and materials
No datasets were generated or analysed during the current study.

Declarations

Competing interests
The authors declare no competing interests.

Received: 29 September 2024 / Accepted: 3 February 2025
Published online: 22 February 2025

References

1. Tsao CW, et al. Heart disease and stroke statistics-2022 update: a Report from the American Heart Association. Circulation. 2022;145(8):e153–639.
2. Anderson JL, Morrow DA. Acute myocardial infarction. N Engl J Med. 2017;376(21):2053–64.
3. Pfeffer MA, Claggett B, Lewis EF, et al. Angiotensin receptor-neprilysin inhibition in acute myocardial infarction. N Engl J Med. 2021;385(20):1845–55.
4. Burke RM, et al. Sacubitril/Valsartan decreases cardiac fibrosis in left ventricle pressure overload by restoring PKG signaling in cardiac fibroblasts. Circ Heart Fail. 2019;12(4):e005565.
5. Ishii M, et al. Cardioprotective effects of LCZ696 (Sacubitril/Valsartan) after experimental acute myocardial infarction. JACC Basic Transl Sci. 2017;2(6):655–68.
6. Liu Y, Zhong C, Si J, Chen S, Kang L, Xu B. The impact of Sacubitril/Valsartan on cardiac fibrosis early after myocardial infarction in hypertensive rats. J Hypertens. 2022;40(9):1822–30.
7. Jin L, Geng L, Ying L, et al. FGF21-Sirtuin 3 axis confers the protective effects of exercise against diabetic cardiomyopathy by governing mitochondrial Integrity. Circulation. 2022;146(20):1537–57.
8. Samuel VT, Shulman GI. Nonalcoholic fatty liver disease as a Nexus of metabolic and hepatic diseases. Cell Metab. 2018;27(1):22–41.
9. Geng L, Lam KSL, Xu A. The therapeutic potential of FGF21 in metabolic diseases: from bench to clinic. Nat Rev Endocrinol. 2020;16(11):654–67.
10. Pan X, et al. FGF21 prevents angiotensin II-Induced hypertension and vascular dysfunction by activation of ACE2/Angiotensin-(1–7) Axis in mice. Cell Metab. 2018;27(6):1323–37. e5.
11. Tang TT, et al. Liver-heart crosstalk controls IL-22 activity in cardiac protection after myocardial infarction. Theranostics. 2018;8(16):4552–62.
12. Sun JY, Du LJ, Shi XR, et al. An IL-6/STAT3/MR/FGF21 axis mediates heart-liver cross-talk after myocardial infarction. Sci Adv. 2023;9(14):eade4110.
13. Youssef J, Badr MZ. PPARs: history and advances. Methods Mol Biol. 2013;952:1–6.
14. Han L, Shen WJ, Bittner S, Kraemer FB, Azhar S. PPARs: regulators of metabolism and as therapeutic targets in cardiovascular disease. Part II: PPAR-β/δ and PPAR-γ. Future Cardiol. 2017;13(3):279–96.
15. Montaigne D, Butruille L, Staels B. PPAR control of metabolism and cardiovascular functions. Nat Rev Cardiol. 2021;18(12):809–23.
16. Schiffrin EL. Peroxisome proliferator-activated receptors and cardiovascular remodeling. Am J Physiol Heart Circ Physiol. 2005;288(3):H1037–43.
17. Qiang L, Accili D. FGF21 and the second coming of PPARgamma. Cell. 2012;148(3):397–8.

18. Fishbein MC, Meerbaum S, Rit J, et al. Early phase acute myocardial infarct size quantification: validation of the triphenyl tetrazolium chloride tissue enzyme staining technique. Am Heart J. 1981;101(5):593–600.
19. Lindsey ML, Bolli R, Canty JM, et al. Guidelines for experimental models of myocardial ischemia and infarction. Am J Physiol Heart Circ Physiol. 2018;314(4):H812–38.
20. Heart Failure Group of Chinese Society of Cardiology of Chinese Medical Association; Chinese Heart Failure Association of Chinese Medical Doctor Association. Editorial Board of Chinese Journal of Cardiology. Zhonghua Xin xue guan bing za zhi. 2018;46(10):760–89.
21. Zhang Y, et al. The role of FGF21 in the pathogenesis of cardiovascular disease. Chin Med J (Engl). 2021;134(24):2931–43.
22. Tan H, Yue T, Chen Z, Wu W, Xu S, Weng J. Targeting FGF21 in cardiovascular and metabolic diseases: from mechanism to medicine. Int J Biol Sci. 2023;19(1):66–88.
23. Zhang W, et al. Serum level of fibroblast growth factor 21 is independently associated with acute myocardial infarction. PLoS ONE. 2015;10(6):e0129791.
24. Bo W, et al. The roles of FGF21 and ALCAT1 in aerobic exercise-induced cardioprotection of postmyocardial infarction mice. Oxid Med Cell Longev. 2021;2021:8996482.
25. Liu SQ, et al. Endocrine protection of ischemic myocardium by FGF21 from the liver and adipose tissue. Sci Rep. 2013;3:2767.
26. Peng S, Lu XF, Qi YD, et al. LCZ696 ameliorates oxidative stress and pressure overload-induced pathological cardiac remodeling by regulating the Sirt3/MnSOD pathway. Oxid Med Cell Longev. 2020;2020:9815039.
27. Shao W, Jin T. Hepatic hormone FGF21 and its analogs in clinical trials. Chronic Dis Transl Med. 2022;8(1):19–25.
28. Pan Q, et al. A novel GLP-1 and FGF21 dual agonist has therapeutic potential for diabetes and non-alcoholic steatohepatitis. EBioMedicine. 2021;63:103202.

Publisher's note